A&A 592, A120 (2016)
DOI: 10.1051/0004-6361/201628864

Astronomy & Astrophysics

Many new variable stars discovered in the core of the globular cluster NGC 6715 (M 54) with EMCCD observations⋆,⋆⋆

R. Figuera Jaimes[1,2], D. M. Bramich[3], N. Kains[6], J. Skottfelt[4,5], U. G. Jørgensen[5], K. Horne[1], M. Dominik[1,⋆⋆⋆], K. A. Alsubai[3], V. Bozza[7,8], M. J. Burgdorf[26], S. Calchi Novati[9,7,10,⋆⋆⋆⋆], S. Ciceri[25], G. D'Ago[10], D. F. Evans[21], P. Galianni[1], S.-H. Gu[12,13], K. B. W Harpsøe[5], T. Haugbølle[5], T. C. Hinse[14], M. Hundertmark[5,1], D. Juncher[5], E. Kerins[29], H. Korhonen[24,15,5], M. Kuffmeier[5], L. Mancini[11], N. Peixinho[27,28], A. Popovas[5], M. Rabus[16,11], S. Rahvar[17], G. Scarpetta[10,7,8], R. W. Schmidt[18], C. Snodgrass[19,20], J. Southworth[21], D. Starkey[1], R. A. Street[22], J. Surdej[23], R. Tronsgaard[30], E. Unda-Sanzana[27], C. von Essen[30], X.-B. Wang[12,13], and O. Wertz[23]
(The MiNDSTEp Consortium)

(Affiliations can be found after the references)

Received 6 May 2016 / Accepted 27 May 2016

ABSTRACT

Context. We show the benefits of using electron-multiplying CCDs and the shift-and-add technique as a tool to minimise the effects of atmospheric turbulence, such as blending between stars in crowded fields, and to avoid saturated stars in the fields observed. We intend to complete, or improve on, the census of the variable star population in globular cluster NGC 6715.
Aims. Our aim is to obtain high-precision time-series photometry of the very crowded central region of this stellar system via the collection of better angular resolution images than has been previously achieved with conventional CCDs on ground-based telescopes.
Methods. Observations were carried out using the Danish 1.54-m telescope at the ESO La Silla observatory in Chile. The telescope is equipped with an electron-multiplying CCD that enables short-exposure-time images to be obtained (ten images per second) that were stacked using the shift-and-add technique to produce the normal-exposure-time images (minutes). The high precision photometry was performed via difference image analysis employing the DanDIA pipeline. We attempted automatic detection of variable stars in the field.
Results. We statistically analysed the light curves of 1405 stars in the crowded central region of NGC 6715 to automatically identify the variable stars present in this cluster. We found light curves for 17 previously known variable stars near the edges of our reference image (16 RR Lyrae and 1 semi-regular) and we discovered 67 new variables (30 RR Lyrae, 21 irregular (long-period type), 3 semi-regular, 1 W Virginis, 1 eclipsing binary, and 11 unclassified). Photometric measurements for these stars are available in electronic form through the Strasbourg Astronomical Data Centre.

Key words. atmospheric effects – instrumentation: high angular resolution – globular clusters: individual: NGC 6715 (M 54) – methods: observational – stars: variables: general – stars: variables: RR Lyrae

1. Introduction

Galactic globular clusters are interesting stellar systems in astronomy since they are fossils of early Galaxy formation and evolution. This makes them excellent laboratories in a wide range of topics from stellar evolution to cosmology, from observations to theory.

NGC 6715 (M 54) was discovered on July 24, 1778 by Charles Messier[1]. The cluster is in the Sagittarius dwarf spheroidal galaxy at a distance of 26.5 kpc from our Sun and 18.9 kpc from our Galactic centre. It has a metallicity [Fe/H] = −1.49 dex and a distance modulus $(m - M)_V$ = 17.58 mag. The magnitude of its horizontal branch is $V_{\rm HB}$ = 18.16 mag (2010 version Harris 1996). The stellar population and morphology of NGC 6715 have attracted the attention of several studies. Although NGC 6715's position is aligned with the central region of the Sagittarius dwarf spheroidal galaxy, recent studies have shown that this cluster is not the nucleus of the mentioned galaxy (Layden & Sarajedini 2000; Majewski et al. 2003; Monaco et al. 2005; Bellazzini et al. 2008). Carretta et al. (2010) found that the metallicity spread in this cluster is intermediate between smaller-normal Galactic globular clusters and metallicity values associated with dwarf galaxies. It has a very peculiar colour−magnitude diagram with multiple main sequences, turnoff points, and an extended blue horizontal branch (HB) (Siegel et al. 2007; Milone 2015). Rosenberg et al. (2004) found that this cluster hosts a blue hook stellar population in its blue HB. It is thought that NGC 6715 might host an intermediate mass black hole (IMBH) in its centre (Ibata et al. 2009; Wrobel et al. 2011) as well.

Oosterhoff (1939) found that globular clusters can be classified into two groups based on the mean periods and the number ratios of their RR0 and RR1 stars. These are the Oosterhoff I (OoI) and Oosterhoff II (OoII) groups, and this is known as the Oosterhoff dichotomy. It was also found that the metallicity of the clusters plays an important role in this classification (Kinman 1959) and that it could be related with the formation history of the Galactic halo (see e.g. discussions in Lee & Carney 1999; Catelan 2004, 2009; Smith et al. 2011; Sollima et al. 2014).

The first Oosterhoff classification for NGC 6715 was done by Layden & Sarajedini (2000) by comparing the amplitudes and periods of 67 RR Lyrae in this cluster with the period-amplitude

⋆ Based on data collected by MiNDSTEp with the Danish 1.54 m telescope at the ESO La Silla observatory.
⋆⋆ Full Table 1 is only available at the CDS via anonymous ftp to cdsarc.u-strasbg.fr (130.79.128.5) or via http://cdsarc.u-strasbg.fr/viz-bin/qcat?J/A+A/592/A120
⋆⋆⋆ Royal Society University Research Fellow.
⋆⋆⋆⋆ Sagan visiting fellow.
[1] http://messier.seds.org/m/m054.html

relation obtained for M3 (OoI) and M9 (OoII). NGC 6715 follows the relation defined by M3 and this implies that it is an OoI cluster. They also found that the mean periods of the RR Lyrae also agree with the OoI classification. Similarly, Sollima et al. (2010), in their study of variable stars in NGC 6715, discovered a new set of 80 RR Lyrae, and they used 95 RR0 and 33 RR1 (after excluding non-members or problematic stars) to find that this cluster shares some properties of both OoI and OoII clusters. For instance, the average period of its RR0 and RR1 stars was found to be intermediate between the values for the OoI and OoII classifications. We note that Catelan (2009) also classified this cluster as an intermediate Oosterhoff type based on its position in the $\langle P_{\rm RR0}\rangle$-metallicity diagram.

Several time-series photometric studies focused on the variable star population (Rosino 1952; Rosino & Nobili 1958; Layden & Sarajedini 2000; Sollima et al. 2010; Li & Qian 2013), but owing to the high concentration of stars in its core, many variables have previously been missed because of blending. NGC 6715 is very massive and it is among the densest known globular clusters (Pryor & Meylan 1993). As a result, NGC 6715 also caught our attention as an excellent candidate for our study of globular clusters using electron-multiplying CCDs (EMCCDs) and the shift-and-add technique (Skottfelt et al. 2013, 2015a; Figuera Jaimes et al. 2016).

Section 2 summarises the observations, the reduction, and photometric techniques employed. Section 3 explains the calibration applied to the instrumental magnitudes. Section 4 contains the technique used in the detection and extraction of variable stars. Sections 5 and 6 show the methodology used to classify variables and the colour−magnitude diagrams employed, respectively. Section 7 presents our results and Sect. 8 discusses the Oosterhoff classification of this cluster. Our conclusions are presented in Sect. 9.

2. Data, reduction, and photometry

EMCCDs, also known as low light level charge-coupled devices (L3CCD; see e.g. Smith et al. 2008; Jerram et al. 2001), are conventional CCDs that have an extended readout register where the signal is amplified by impact ionisation before they are read out. Hence the readout noise is negligible when compared to the signal and very high frame-rates become feasible (10−100 frames/s). This provides an opportunity to compensate for the blurring effect of the turbulence in the atmosphere. By shifting and adding the individual frames appropriately, it is possible to construct much higher resolution images than is possible using conventional CCD imaging from the ground. Furthermore, the dynamic range of the stacked images is greatly increased and the saturation of bright stars is therefore not an issue except for the very brightest stars in the sky. However, the main drawback with this technique is that the process, whereby the signal is amplified, also increases the photon noise component in the images by a factor of $\sqrt{2}$, when compared to conventinal CCD images. We also need to be aware that EMCCD imaging data need to be calibrated in a different way to conventional CCD data. Several studies where EMCCDs have been used can be found in the literature, e.g. high-resolution imaging of exoplanet host stars in the search for unseen companions (Southworth et al. 2015; Ciceri et al. 2016; Bozza et al. 2016; Street et al. 2016; Evans et al. 2016) photometric and astrometric measurements of a pair of very close brown dwarfs (Mancini et al. 2015), and time-series photometry of crowded globular cluster cores aiming to complete the census of variable stars (Skottfelt et al. 2015a; Figuera Jaimes et al. 2016).

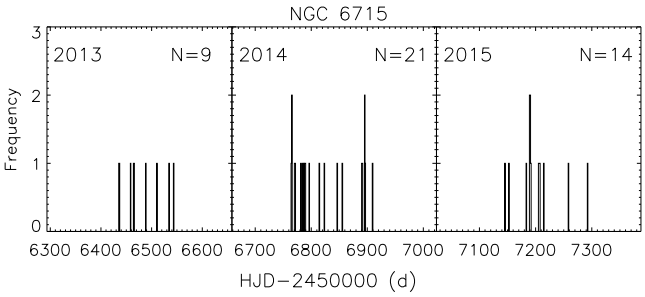

Fig. 1. Histograms with the number of observations per night for globular cluster NGC 6715. *Left*: 2013. *Middle*: 2014. *Right*: 2015.

The data presented in this paper are the result of EMCCD observations performed over three consecutive years: 2013, 2014, and 2015 in April to September each year. The 1.54 m Danish telescope at the ESO Observatory in La Silla, Chile was used with an Andor Technology iXon+897 EMCCD camera, which has a 512 × 512 array of 16 μm pixels, giving a pixel scale of ∼0.″09 per pixel and a total field of view of ∼45 × 45 arcsec^2.

For this research, the EMCCD camera was set to work at a frame-rate of 10 Hz (ten frames per second) and an EM gain of 300e^-/photon. The camera was placed behind a dichroic mirror which works as a long-pass filter. Taking the mirror and the sensitivity of the camera into consideration, it is possible to cover the wavelength range from 650 nm to 1050 nm. This is roughly a combination of SDSS $i' + z'$ filters (Bessell 2005). More details about the instrument can be found in Skottfelt et al. (2015b). The total exposure time employed for a single observation was ten minutes, which means that each observation is the result of shifting-and-adding 6000 exposures. The resulting point spread function (PSF) full width at half maximum (FWHM) in the reference image employed in the photometric reductions (see below) was 0.44″, while the mean standard seeing calculated with the values reported at the observatory station during April to September 2013, 2014, and 2015 were 1.0″, 1.2″, and 0.9″, respectively.

In Fig. 1, histograms of the number of observations per night during each year are shown. Data in the left-hand panel correspond to 2013, data in the middle panel to 2014, and data in the right-hand panel to 2015. We aimed to always take two observations per night, although it was not always possible because of weather conditions or time slots needed for other projects, as is the case of the monitoring of microlensing events carried out by the MiNDSTEp consortium.

Bias, flat-field, and tip-tilt corrections were performed using the procedures and algorithms described in Harpsøe et al. (2012). In particular, the tip-tilt correction allows high-resolution stacked images to be created, as described in detail in Skottfelt et al. (2015a), Figuera Jaimes et al. (2016). Briefly, the method uses the Fourier cross-correlation theorem where, for each bias- and flat-corrected exposure $I_k(i, j)$ within an observation, we calculate the cross-correlation image between $I_k(i, j)$ and an average of 100 randomly chosen exposures. The peak in the cross-correlation image gives the appropriate shift to correct the tip-tilt error. We then stack the shifted exposures according to batches grouped by image quality (a measure of image sharpness), to create ten-layer image cubes. The best quality layers from each cube (i.e. the sharpest layers) are extracted from all of the available observations to create a high-resolution reference image for subsequent difference image analysis (DIA). Finally, each ten-layer cube is stacked to create a single image that corresponds to each observation.

Table 1. Time-series *I*-band photometry for all known and new variables in the field of view covered in globular cluster NGC 6715.

var id	Filter	HJD	$M_{\rm std}$	$m_{\rm ins}$	σ_m	$f_{\rm ref}$	$\sigma_{\rm ref}$	$f_{\rm diff}$	$\sigma_{\rm diff}$	p
		(d)	(mag)	(mag)	(mag)	($\rm ADUs^{-1}$)	($\rm ADUs^{-1}$)	($\rm ADUs^{-1}$)	($\rm ADUs^{-1}$)	
(1)	(2)	(3)	(4)	(5)	(6)	(7)	(8)	(9)	(10)	(11)
V112	I	2 456 435.88824	13.706	4.679	0.001	141 855.480	1550.259	–44401.153	540.539	5.9879
V112	I	2 456 436.89695	13.689	4.661	0.001	141 855.480	1550.259	–30447.356	609.851	5.8368
⋮	⋮	⋮	⋮	⋮	⋮	⋮	⋮	⋮	⋮	⋮
V160	I	2 456 435.88824	17.882	8.855	0.012	4069.406	1553.328	–7171.335	186.330	5.9879
V160	I	2 456 436.89695	17.646	8.618	0.015	4069.406	1553.328	–2916.178	292.135	5.8368
⋮	⋮	⋮	⋮	⋮	⋮	⋮	⋮	⋮	⋮	⋮
V173	I	2 456 435.88824	17.745	8.717	0.011	3251.773	1764.129	+39.643	192.483	5.9879
V173	I	2 456 436.89695	17.770	8.743	0.017	3251.773	1764.129	–400.238	286.082	5.8368
⋮	⋮	⋮	⋮	⋮	⋮	⋮	⋮	⋮	⋮	⋮

Notes. The standard $M_{\rm std}$ and instrumental $m_{\rm ins}$ magnitudes are listed in Cols. 4 and 5, respectively, corresponding to the variable star, filter, and epoch of mid-exposure listed in Cols. 1–3, respectively. The uncertainty on $m_{\rm ins}$ is listed in Col. 6, which also corresponds to the uncertainty on $M_{\rm std}$. For completeness, we also list the quantities $f_{\rm ref}$, $f_{\rm diff}$, and p from Eq. (2) in Cols. 7, 9, and 11, along with the uncertainties $\sigma_{\rm ref}$ and $\sigma_{\rm diff}$ in Cols. 8 and 10. This is an extract from the full table, which is available at the CDS.

To extract the photometry in each of the stacked images, we used the DanDIA[2] pipeline (Bramich 2008; Bramich et al. 2013), which is based on difference image analysis (DIA; Alard & Lupton 1998; Alard 2000). The pipeline works by aligning all images to the reference image, solving for a set of convolution kernels that were modelled as discrete pixel arrays, and subtracting the convolved reference image in each case to create a set of difference images. Stars are detected on the reference image and their reference fluxes $f_{\rm ref}$ (ADU/s) are measured using PSF photometry. Difference fluxes $f_{\rm diff}(t)$ (ADU/s) for each star detected in the reference image are measured in each of the difference images by optimally scaling the PSF model for the star to the difference image. The light curve for each star in instrumental magnitudes $m_{\rm ins}$ are built as shown in Eq. (1):

$$m_{\rm ins}(t) = 17.5 - 2.5\log(f_{\rm tot}(t)), \quad (1)$$

where $f_{\rm tot}(t)$ is the total flux in ADU/s defined as

$$f_{\rm tot}(t) = f_{\rm ref} + \frac{f_{\rm diff}(t)}{p(t)}. \quad (2)$$

The quantity $p(t)$ is the photometric scale factor used to scale the reference frame to each image, as part of the kernel model explained in Bramich (2008). An electronic table with photometric measurements and fluxes for all the variable stars presented in this work is available through the CDS[3] database with the format illustrated in Table 1.

2.1. Astrometry and a finding chart

To create a reference image with the astrometric information for each star in the field covered in NGC 6715, we used the celestial coordinates available in the ACS Globular Cluster Survey[4] (see Anderson et al. 2008), which were uploaded for the field of the cluster through GAIA (Graphical Astronomy and Image Analysis Tool; Draper 2000). An (x, y) shift to match their respective stars in our reference image was applied. Stars lying outside the field of view and those without a clear match were removed and the (x, y) shift was refined by minimising the squared coordinate residuals. A total of 305 stars over the entire field was used to guarantee that the astrometric solution applied to the reference image considered enough stars. The radial root mean square (rms) scatter obtained in the residuals was ∼0.″028 (∼0.3 pixels). This astrometrically calibrated reference image was used to produce a finding chart for NGC 6715 on which we marked the positions and identifications of all variable stars studied in this work (Fig. 5). Finally, a table with the equatorial J2000 celestial coordinates of all variables is given in Table A.1.

3. Photometric calibration

The photometric transformation of instrumental magnitudes to the standard system was accomplished using information available in the ACS Globular Cluster Survey, which provides calibrated magnitudes for selected stars in the fields of 50 globular clusters extracted from images taken with the *Hubble* Space Telescope (HST) instruments ACS and WFPC.

By matching the positions of the stars in the field of the HST images with those in our reference image, we obtained the photometric transformation shown in Fig. 2. The I magnitude obtained from the ACS (see Siegel et al. 2007) is plotted versus the instrumental $i' + z'$ magnitude obtained in this study. The red line is a linear fit with slope unity yielding the zero point labelled in the title, where N is the number of stars used in the fit and R is the correlation coefficient obtained. Owing to the substantial differences between the $i' + z'$ and standard I wavebands, there are non-linear colour terms in the transformation that we have not accounted for. However, we have opted for an approximate absolute photometric calibration since variable star discovery and classification do not require a precise calibration. Furthermore, our non-standard $i' + z'$ waveband precludes the possibility of using our RR Lyrae light curves for physical parameter estimation.

4. Variable star searches

Light curves for a total of 1405 stars were obtained with the DanDIA pipeline in the field covered by the reference image. To detect and extract the variable stars from all the non-variables,

[2] DanDIA is built from the DanIDL library of IDL routines available at http://www.danidl.co.uk
[3] http://cds.u-strasbg.fr/
[4] http://www.astro.ufl.edu/~ata/public_hstgc/

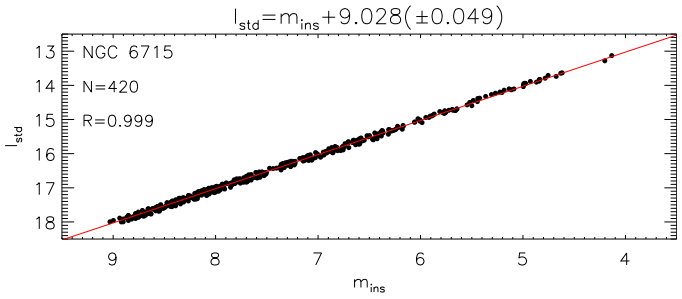

Fig. 2. Standard I magnitude taken from the HST observations as a function of the instrumental $i' + z'$ magnitude. The red line is the fit that best matches the data and it is described by the equation in the title. The correlation coefficient is 0.999.

three automatic (or semi-automatic) techniques were employed. They are described in Sects. 4.1–4.3.

4.1. Root mean square

A diagram of root mean square (rms) magnitude deviation against mean I magnitude (see top Fig. 3) was constructed for the cluster. In this diagram, we measure not only the photometric scatter for each star, but also the intrinsic variation of the variable stars over time, which gives them a higher rms than the non-variables. The classification is indicated by the colour as detailed in Table 2. To select candidate variable stars, we fit a polynomial to the rms values as a function of magnitude and flag all stars with an rms greater than two times the model value.

4.2. S_B statistic

A detailed discussion can be found about the benefits of using the S_B statistic to detect variable stars (Figuera Jaimes et al. 2013) and RR Lyrae with Blazhko effect (Arellano Ferro et al. 2012). The S_B statistic is defined as

$$S_B = \left(\frac{1}{NM}\right)\sum_{i=1}^{M}\left(\frac{r_{i,1}}{\sigma_{i,1}} + \frac{r_{i,2}}{\sigma_{i,2}} + \ldots + \frac{r_{i,k_i}}{\sigma_{i,k_i}}\right)^2, \quad (3)$$

where N is the number of data points for a given light curve and M is the number of groups formed of time-consecutive residuals of the same sign from a constant-brightness light curve model (e. g. "mean or median"). The residuals $r_{i,1}$ to r_{i,k_i} correspond to the ith group of k_i time-consecutive residuals of the same sign with corresponding uncertainties $\sigma_{i,1}$ to σ_{i,k_i}. The S_B statistic is larger in value for light curves with long runs of consecutive data points above or below the mean, which is the case for variable stars with periods longer than the typical photometric cadence.

A plot of S_B versus mean I magnitude is given for NGC 6715 (see bottom Fig. 3), variable stars are plotted in colour. To select candidate variable stars, the same technique employed in Sect. 4.1 was used, with the threshold also set at two times the model S_B values.

4.3. Stacked difference image

Based on the results obtained using the DanDIA pipeline, a stacked difference image was built for NGC 6715 with the aim of detecting the difference fluxes that correspond to variable stars in the field of the reference image. The stacked image is the result of summing the absolute values of the difference images divided by the respective pixel uncertainty

$$S_{ij} = \sum_k \frac{|D_{kij}|}{\sigma_{kij}}, \quad (4)$$

where S_{ij} is the stacked image, D_{kij} is the kth difference image, σ_{kij} is the pixel uncertainty associated with each image k, and the indexes i and j correspond to pixel positions.

All of the variable star candidates obtained by using the rms and S_B diagrams explained in Sects. 4.1 and 4.2 were inspected visually in the stacked image and by blinking the difference images to confirm or refute their variability.

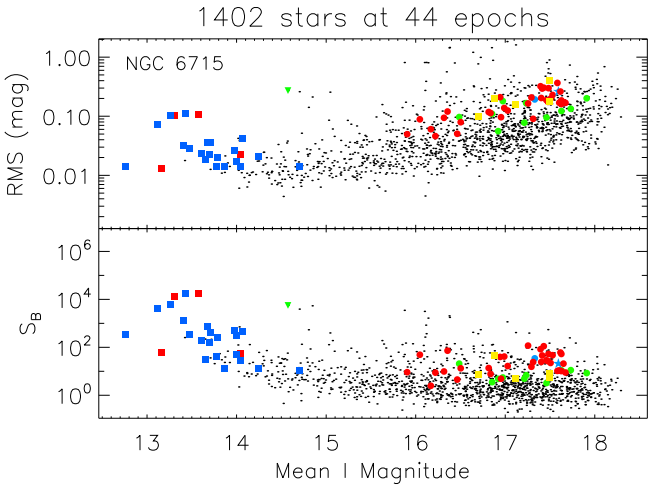

Fig. 3. Root mean square (rms) magnitude deviation (*top*) and S_B statistic (*bottom*) versus the mean I magnitude for the 1402 stars detected in the field of view of the reference image for NGC 6715. Coloured points follow the convention adopted in Table 2 to identify the types of variables found in the field of this globular cluster.

Table 2. Convention used in the variable star classification of this work based on the definitions of the General Catalogue of Variable Stars (Samus et al. 2009).

Type	Id	Point style	Color
Pulsating Variables			
RR Lyrae	RR0	Filled circle	Red
	RR1	Filled circle	Green
	RR01	Filled circle	Blue
W Virginis	CWA	Inverted triangle	Green
Semi-regular	SR	Filled square	Red
Long-period irregular	L	Filled square	Blue
Eclipsing Binaries			
In general	E	Five pointed star	Blue
Unclassified Variables			
In general	NC	Filled square	Yellow

5. Variable star classification

To define the type of variation in each of the variable stars found, several steps were done. First, we used their position in the colour−magnitude diagram (CMD; Fig. 4) as a reference for their evolutionary stage as most types of variable stars are placed in very well defined zones in the CMD. Second, we implemented a period search for each of the light curves by using the string

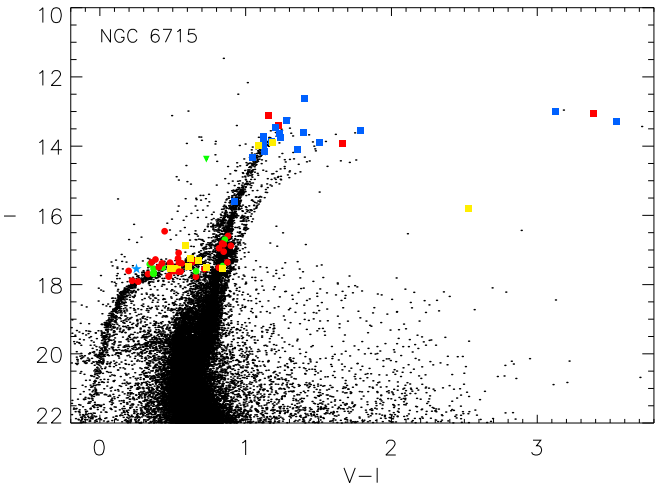

Fig. 4. Colour magnitude diagram of the globular cluster NGC 6715 built with V and I magnitudes available in the ACS globular cluster survey extracted from HST images.

method (Lafler & Kinman 1965) and by minimising the χ^2 in a Fourier analysis fit. Periods found and light curve shapes were also taken into account. Finally, to classify the variable stars, we used the conventions defined in the General Catalogue of Variable Stars (Samus et al. 2009).

In Table 2, the classification, corresponding symbols, and colours used in the plots throughout the paper are shown.

6. Colour magnitude diagram

Since our sample only has data available for one filter, we decided to build the colour−magnitude diagram (CMD; see Fig. 4) by using the information available from the HST images at the ACS Globular Cluster Survey. The data used correspond to the V and I photometry obtained in Sirianni et al. (2005). The CMD was useful in classifying the variable stars, especially those with poorly defined light curves such as long period variables and semi-regular variables, as well as corroborating cluster membership.

7. NGC 6715/C1851-305/Messier 54

The details of all variable stars in our FoV that are discussed in this section are listed in Table A.1, and all light curves are plotted in Fig. A.1.

7.1. Known variables

This globular cluster has of the order of 200 known variable stars listed in the Catalogue of Variable Stars in Galactic Globular Clusters (CVSGGC; Clement et al. 2001). Most of them are of the RR Lyrae type but a few are irregular (long-period type), semi-regular, W Virginis, eclipsing binaries, and SX Phoenicis. To date, four studies report variable star discoveries in this globular cluster: V1-V28 from Rosino (1952), V29-V82 from Rosino & Nobili (1958), V83-V117 from Layden & Sarajedini (2000), and V118-V211 from Sollima et al. (2010).

In the field of view covered by our reference image there are only five known variable stars (V112, V160, V173, V181, V192). All of them lie towards the edges of the image, as can be seen in Fig. 5. The star V112 was previously classified as irregular. However, we were able to find a period of ∼100 days in the variability of this star and, because of this, we reclassified it as a semi-regular variable. For V160, we were not able to produce a good phased light curve using the published period of 0.6194848 d. The discovery observations by Sollima et al. (2010) cover a time baseline of only six days. With our time baseline of more than two years, our derived periods are much more precise and the period found is in agreement with that found by the Optical Gravitational Lensing Experiment (OGLE, Udalski et al. 1992; Soszyński et al. 2014, see below). For V160, we list the OGLE period of 0.62813716 d in Table A.1. For V173, we improved the period estimate over that from Sollima et al. (2010). For V181, we find a very different period with respect to the one estimated by Sollima et al. (2010). The new period of 0.877072 d makes this RR Lyrae the one with the longest period in the cluster. The phased light curve in Fig. A.1 is somewhat noisy because this variable is highly blended with a brighter star. The case of V192 is particularly interesting because the star was classified as RR1 with a period of 0.3986799 d. However, at the astrometric position reported for this star we found a RR Lyrae type RR0 with a period of 0.600373 d. This is also in agreement with the period and classification found by OGLE (see below), which we list in Table A.1. Again, the phased light curve of this variable is noisy because of blending with a brighter star. It is clear then that the Sollima et al. (2010) periods and RR Lyrae classifications are not robust based on relatively few observations. We discuss the consequences of this later on.

Recently, Montiel & Mighell (2010) announced 50 RR Lyrae candidates based on observations taken with the HST. However, the data obtained consist of 12 epochs covering only 8 hours, which made the study unsuitable for a period search and certainly some RR Lyrae stars will have been missed with such a short time baseline. No light curves were presented in their paper. Of these 50 candidate variable stars, 17 lie outside of our field of view (VC2, VC11-VC18, VC22, VC24, VC38, VC44, VC45, VC47-VC49). As pointed out in the Catalogue of Variable Stars in Galactic Globular Clusters (Clement et al. 2001), 11 of these candidates are previously known variables, thus VC2 = V127, VC11 = V162, VC12 = V163, VC13 = V95, VC14 = V164, VC15 = V142, VC17 = V129, VC18 = V179, VC44 = V46, VC45 = V148, and VC47 = V76 (see also Appendix B). For eight of their candidates in our field of view, we could not detect variations in our difference images at their coordinates (VC3, VC6, VC19, VC21, VC29, VC42, VC43, VC50), and we therefore cannot confirm their variability. We plot their positions in Fig. 5 with a green square[5]. Three of their candidates in our field of view, VC28, VC34, and VC46, are the known variables V181, V160, and V192, respectively. We confirm the variable nature of the remaining 22 candidates in our field of view, and we have assigned them "V" numbers as part of our study (see Sect. 7.2). Table A.1 lists their VC identification in Col. 2. We classify 18 of them as RR Lyrae stars, one as an eclipsing binary, and are unable to classify VC27, VC32, and VC33. We plot their positions in Fig. 5 with a square symbol.

The study by McDonald et al. (2014) using the *VISTA* survey also covered the cluster and presents candidate variables based on typically ∼12−13 epochs spread over ∼100−200 days, which was insufficient to derive periods for many of them. Of the short period candidate variables listed in their Table 1, 18 are inside the field of view covered by our reference image. None of the bright irregular variables listed in their Table 2 and

[5] The Montiel & Mighell (2010) coordinates differ by RA ∼ 0.3″ and Dec ∼0.8″ from our coordinates and we have corrected for this in Fig. 5.

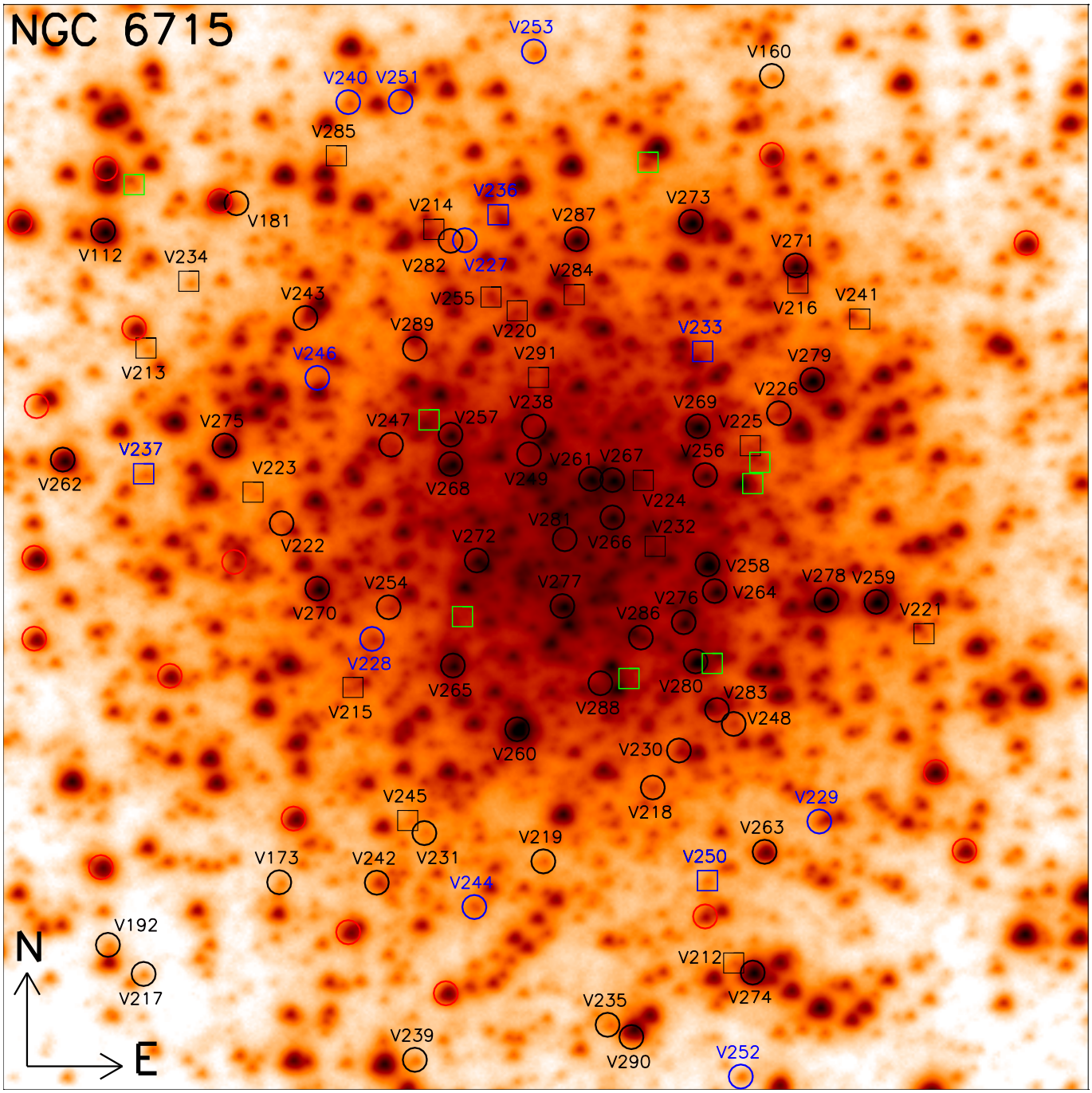

Fig. 5. Finding chart for the globular cluster NGC 6715. The image used corresponds to the reference image constructed during the reduction. All known variables and new discoveries are labelled with their V numbers. Known variables, or new variables discovered in this work, are plotted with black symbols. Variables discovered by the OGLE survey are plotted with blue symbols. Those variables that were candidate variables from Montiel & Mighell (2010) are plotted using squares. Otherwise symbols are circles. Green squares and red circles, both without labels, are candidate variables from Montiel & Mighell (2010) and McDonald et al. (2014), respectively, for which we do not detect variability in our survey. Image size is $\sim 40 \times 40$ arcsec^2.

faint candidates listed in their Table 3 are inside the field covered in our study. Positions of these stars inside our field of view are plotted in Fig. 5 with a red circle. It is worth noting that all of these candidates are located more toward the edges of the reference image. We detect variability in only two of the McDonald et al. (2014) candidates within our field of view (SPVSgr18550405-3028580 and SPVSgr18550386-3028593, which we assign *V* identifications as V229 and V263, respectively, see Sect. 7.2).

Similarly, the field of this cluster was also covered by OGLE, particularly with their OGLE-IV survey (Soszyński et al. 2014; Udalski et al. 2015). In this survey, we find 15 of the variable stars studied in our work, of which two are previously known variables (V160 and V192), and 13 are new discoveries by OGLE (we assigned the following *V* identifications: V227-V229, V233, V236, V237, V240, V244, V246, V250-V253). The OGLE light curves for these stars typically have $\sim$150 epochs covering a baseline of $\sim$2.5 yrs and OGLE derived

precise periods for them. With our data, we were also able to find the same periods and type of classification assigned by OGLE. The positions of these stars are plotted in Fig. 5 with a blue colour. Again, it is worth noting that all of these variables are located more toward the edges of the reference image. In the particular case of V229, V244, and V246, the pipeline was not able to detect these stars in the reference image but their variation is clear in the difference images. Their differential fluxes against phase are plotted in Fig. A.1. Finally, epochs, periods, mean magnitudes, amplitudes, and classifications for these three stars were taken from the OGLE database, although the number of data points listed in Table A.1 correspond to our light curves.

In Appendix B (Table B.1), we provide the cross-identifications for the previously known RR Lyrae stars in NGC 6715 between the CVSGGC (Clement et al. 2001), the variable star candidates from Montiel & Mighell (2010), and the OGLE RR Lyrae stars (Soszyński et al. 2014).

7.2. New variables

After employing the methods described in Sect. 4, we were able to extract 67 new variable stars in the core of NGC 6715 of which 30 are RR Lyrae, one is a W Virginis star (CWA), 21 are irregular (long-period type), three are semi regular, one is an eclipsing binary, and 11 remain without classification.

7.2.1. RR Lyrae

V213-V226, V230-V232, V234-V235, V238-V239, V241-V243, V245, V247-V249, V254-V255: these 30 newly discovered variable stars are clear RR Lyrae variables. Their positions in the CMD, light curve shapes, periods, and amplitudes corroborate their variability type. We found that 17 are pulsating in the fundamental mode (RR0); eight are pulsating in the first overtone (RR1); one is a double-mode pulsator (RR01) and four RR Lyrae remain with an uncertain subtype (3 RR0? and 1 RR1?). As shown in Table A.1, their periods range from ∼0.28 d to ∼0.76 d, with amplitudes between 0.06 and 1.69 mag.

The periodogram analysis for V221 showed two predominant frequencies typical of double mode RR Lyrae stars, one equivalent to the fundamental period $P_0 = 0.459608$ d, and one equivalent to the first overtone period $P_1 = 0.343828$ d giving a period ratio $P_1/P_0 = 0.748$, which falls into the expected ratio range of ∼0.725 to ∼0.748 for this type of pulsating RR Lyrae stars (Netzel et al. 2015; Moskalik 2013; Cox et al. 1983). Further data for a more detailed analysis of this star will be useful to corroborate its pulsational properties.

7.2.2. W Virginis

V256: particularly interesting is the case of this star, since its variation (and position in the CMD) do not follow the pattern found for the other variable stars studied and classified in this work. We found a very well phased light curve with a period of ∼14.771 d and an amplitude of 0.71 mag. This is the only bright variable star on the blue side of the colour−magnitude diagram far away from the red giant branch.

The properties found in the variation of this star and its position in the CMD match very well with the W Virginis-type of variable star described in Samus et al. (2009), particularly with the subtype CWA, which has periods longer than eight days (see also Wallerstein 2002). Although these types of stars have not been commonly found in globular clusters in contrast to RR Lyrae stars, they are not entirely uncommon. In the statistics of variable stars in Galactic globular clusters reported by Clement et al. (2001), it is possible to notice that 60 variable stars are Cepheids, which include Population II Cepheids, anomalous Cepheids, and RV Tauri stars. V256 is the first CWA star discovered in this cluster.

7.2.3. Irregular

V260-V280: these 21 stars are located at the top of the red giant branch, as shown with blue squares in Fig. 4. Their amplitudes range from 0.05 to 0.46 mag. We found no clear periods for these stars. Owing to this and also their position in the colour−magnitude diagram, we classified them as irregular. Light curves for all these variables are found in Fig. A.1.

7.2.4. Semi regular

V257-V259: based on the position of these three stars in the colour−magnitude diagram (see Fig. 4), their periods, and the shape of their light curves, we have classified them as semi-regular. Light curves for these variables may be found in Fig. A.1. Their amplitudes range from ∼0.04 to ∼0.45 mag and their periods span between ∼20 and ∼150 d.

7.2.5. Eclipsing binary

V212: the light curve variations for this star are very similar to those presented in eclipsing binary systems. We found that the amplitude of the deeper eclipse is of the order of ∼0.8 mag and the amplitude of the secondary eclipse is ∼0.5 mag. The phased light curve shown in Fig. A.1 represented a period of $P = 0.202144$ d.

7.2.6. Other variable stars

V281-V285: these five stars are clear variable stars. They show clear variability by blinking the difference images. They have amplitudes between 0.45 and 0.94 mag. Several attempts to determine periods for these stars were done without success. As a result, their light curves in Fig. A.1 are plotted against HJD. We note that the variable source V281 is only ∼0.24 arcsec from the photometric centre of the cluster, as measured by Goldsbury et al. (2010).

V286: towards the beginning of the 2013 data, we found that the flux of this star was increasing to a maximum at ∼2 456 464.9081 d of about ∼39 400 ADU/s on the flux scale of the reference image, corresponding to a peak magnitude of ∼15.04 mag. After that, its flux strongly decreased during the rest of the observational campaign. During 2014 and 2015, we found that the object seems to be at baseline and it is not detected in the original images.

The centre of NGC 6715 is ∼4.45 arcseconds from this source. Also, at a distance of 3.73 arcseconds, there is an X-ray source studied by Wrobel et al. (2011) using data from *Chandra* and *Hubble* Space Telescope. Given the relatively small astrometric uncertainties in these positions, V286 is not associated with either. The nature and classification of this variable will need further studies, and it will remain without classification in this work.

V287-V291: these five stars were not detected by the pipeline in the reference image. Unfortunately, there are no light curves available in the OGLE database for these stars, but their

variations are clear in the difference images. In Fig. A.1 their differential fluxes against HJD are plotted. As we were not able to produce phased light curves for them, they will remain without classification until future studies are done.

8. Oosterhoff dichotomy

In this work, we discovered 30 new RR Lyrae, and OGLE also discovered 17 more (of which 13 are inside our FoV). After removing the stars without a secure classification, there are 33 new RR0 and nine new RR1 stars, which represent a significant increment in the known RR Lyrae population. The vast majority of these new RR Lyrae stars are cluster members since we have studied the core of NGC 6715. Hence it is pertinent to recalculate the mean periods and number ratios of the RR Lyrae stars to see if they modify the current conclusions about the Oosterhoff type of NGC 6715.

However, we note that NGC 6715 lies projected against the Sagittarius dwarf spheroidal galaxy and behind the Galactic bulge. Therefore, the sample of RR Lyrae stars in the field of the cluster is a mixture of cluster members, bulge stars, and Sagittarius dwarf spheroidal (Sgr dSph) stars. Towards the centre of NGC 6715, the cluster member RR Lyraes dominate, but limiting our sample to the cluster core also reduces the number of RR Lyraes that can be used to calculate the mean periods and number ratios. Hence, in Fig. 6, we have plotted the total number of RR Lyrae stars, the mean period of the RR0 stars, the mean period of the RR1 stars, and the number ratio of the RR1 to all RR Lyrae stars (nRR1/(nRR0 + nRR1)), all as a function of distance from the cluster centre (RA(J2000) = 18:55:03.33; Dec(J2000) = −30:28:47.5; Goldsbury et al. 2010). To convert angles on the sky into distances in parsecs, we used the distance from the Sun to NGC 6715 of 26500 pc (Harris 1996, 2010 version). The inner and outer red vertical lines are the tidal radii estimated by McLaughlin & van der Marel (2005) based on King (1966) and Wilson (1975) models, respectively. The horizontal black lines correspond to the OoI (solid) and OoII (dashed) types given by (Smith 1995) in his Table 3.2. We only used RR Lyrae stars with certain classifications (i.e. published phased light curves with reliable period estimates).

Figure 6 clearly shows that within the range of the two estimates of the tidal radii, where the RR Lyrae stars from the cluster still dominate, the values of $\langle P_{\rm RR0}\rangle$, $\langle P_{\rm RR1}\rangle$ and nRR1/(nRR0 + nRR1) are intermediate between those expected for OoI and OoII clusters. We obtain $\langle P_{\rm RR0}\rangle$ = 0.613529 d, $\langle P_{\rm RR1}\rangle$ = 0.334107 d, and nRR1/(nRR0 + nRR1) = 0.24050633 when calculated for the 79 RR Lyraes within the outer estimate of the tidal radius (i.e. 380 pc). The contaminating RR Lyrae populations have ($\langle P_{\rm RR0}\rangle$, $\langle P_{\rm RR1}\rangle$) = (0.556 d, 0.310 d) and ($\langle P_{\rm RR0}\rangle$,$\langle P_{\rm RR1}\rangle$) = (0.574 d, 0.322 d) for the bulge and Sgr dSph, respectively (Soszyński et al. 2011; Cseresnjes 2001), placing them in the OoI region in the $\langle P_{\rm RR0}\rangle$-metallicity diagram of Catelan (2009). This explains why the values of $\langle P_{\rm RR0}\rangle$ and nRR1/(nRR0 + nRR1) tend towards the OoI values beyond the outer estimate of the tidal radius. The value of $\langle P_{\rm RR1}\rangle$ is hardly influenced though, because there are only six RR1 stars beyond the outer estimate of the tidal radius. Hence the new RR Lyrae discoveries in this paper have served to confirm that NGC 6715 is of intermediate Oosterhoff type.

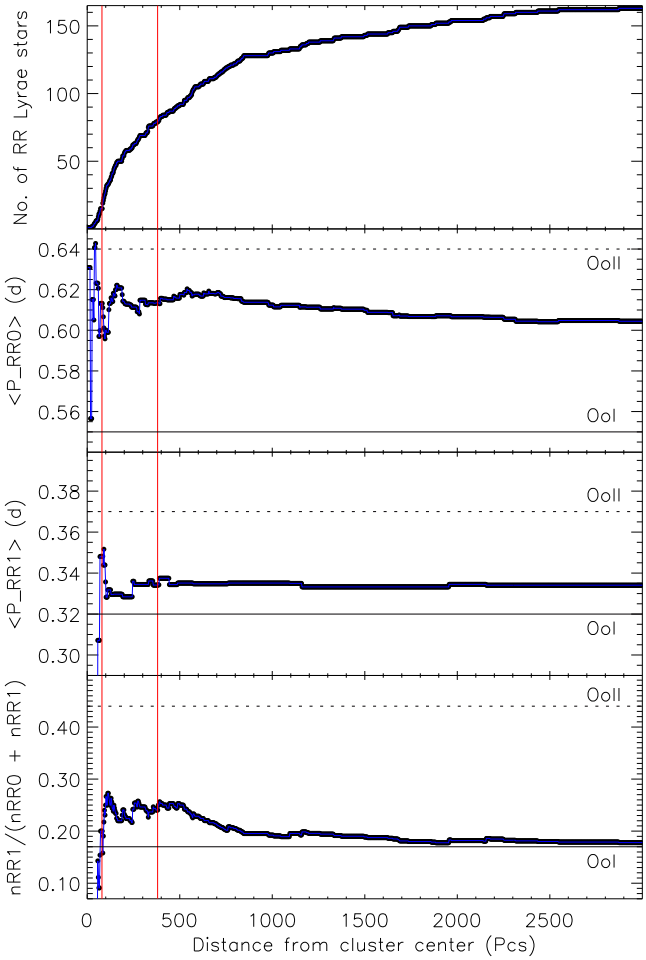

Fig. 6. The number of RR Lyraes, mean periods, and number ratios as a function of the distance from the cluster centre. The red lines correspond to the tidal radii calculated by McLaughlin & van der Marel (2005).

9. Conclusions

The globular cluster NGC 6715 turns out to be a very interesting stellar system, for which images with the highest angular resolution have ever been obtained so far with ground-based telescopes. The use of the EMCCD and shift-and-add technique was demonstrated to be an excellent procedure to minimise the effect of the atmospheric turbulence, which is one of the main constraints when doing ground-based observations. Thanks to this and the use of difference image analysis, it was possible to obtain high-precision time series photometry in the core of this cluster down to $I \sim 18.3$ mag.

A total of 1 405 stars in the field covered by the reference image were statistically studied for variable star detection. We presented light curves for 17 previously known variables that were found toward the edges of the reference image (16 RR Lyrae and 1 SR). We also discovered 67 new variable stars, which consist of 30 RR Lyrae, 21 irregular (long-period type), three semi-regular, 1 W Virginis, one eclipsing binary, and 11 unclassified stars. We estimated periods and ephemerides for all variable stars in the field of our reference image. Our new RR Lyrae star discoveries help confirm that NGC 6715 is of intermediate Oosterhoff type. Finally, our photometric measurements for all variable stars studied in this work are available in electronic form through the Strasbourg Astronomical Data Centre.

Acknowledgements. Our thanks go to Christine Clement for clarifying the known variable star content in NGC 6715 and the numbering systems of the variable stars while we were working on these clusters. This support to the astronomical community is very much appreciated. The Danish 1.54 m telescope is operated based on a grant from the *Danish Natural Science Foundation (FNU)*.

This publication was made possible by NPRP grant # X-019-1-006 from the *Qatar National Research Fund (a member of Qatar Foundation)*. The statements made herein are solely the responsibility of the authors. K.H. acknowledges support from STFC grant ST/M001296/1. G.D. acknowledges Regione Campania for support from POR-FSE Campania 2014-2020. D.F.E. is funded by the UK Science and Technology Facilities Council. T.H. is supported by a Sapere Aude Starting Grant from the Danish Council for Independent Research. Research at Centre for Star and Planet Formation is funded by the Danish National Research Foundation. T.C.H. acknowledges support from the Korea Research Council of Fundamental Science & Technology (KRCF) via the KRCF Young Scientist Research Fellowship. Programme and for financial support from KASI travel grant number 2013-9-400-00, 2014-1-400-06 & 2015-1-850-04. N.P. acknowledges funding by the Gemini-Conicyt Fund, allocated to project No. 32120036 and by the Portuguese FCT – Foundation for Science and Technology and the European Social Fund (ref: SFRH/BGCT/113686/2015). CITEUC is funded by National Funds through FCT – Foundation for Science and Technology (project: UID/Multi/00611/2013) and FEDER – European Regional Development Fund through COMPETE 2020 – Operational Programme Competitiveness and Internationalisation (project: POCI-01-0145-FEDER-006922). OW and J. Surdej acknowledge support from the Communauté française de Belgique – Actions de recherche concertées – Académie Wallonie-Europe. This work has made extensive use of the ADS and SIMBAD services, for which we are thankful.

Note added in proof. During the final stages of the refereeing process for this paper, Hamanowicz et al. (2016) posted a draft paper on the arXiv preprint website on the subject of variable stars in Sgr dSph and M 54. They used OGLE imaging data with conventional CCDs, covering a much larger field of view than our work, although our images are of better resolution having been obtained with EMCCDs. While both sets of results are complementary, there are however a substantial number of variables that have been independently discovered by ourselves and Hamanowicz et al. (2016). These stars are indicated in Col. 2 of Table A.1 with the term O16. Both teams agreed to work together to form a consistent naming convention for the new variable stars with the aim of avoiding confusion for future researchers. We believe that the positive scientific spirit shown by both teams to solve this issue to the benefit of the astronomical community is commendable.

References

Alard, C. 2000, A&AS, 144, 363
Alard, C., & Lupton, R. H. 1998, ApJ, 503, 325
Anderson, J., Sarajedini, A., Bedin, L. R., et al. 2008, AJ, 135, 2055
Arellano Ferro, A., Bramich, D. M., Figuera Jaimes, R., Giridhar, S., & Kuppuswamy, K. 2012, MNRAS, 420, 1333
Bellazzini, M., Ibata, R. A., Chapman, S. C., et al. 2008, AJ, 136, 1147
Bessell, M. S. 2005, ARA&A, 43, 293
Bozza, V., Shvartzvald, Y., Udalski, A., et al. 2016, ApJ, 820, 79
Bramich, D. M. 2008, MNRAS, 386, L77
Bramich, D. M., Horne, K., Albrow, M. D., et al. 2013, MNRAS, 428, 2275
Carretta, E., Bragaglia, A., Gratton, R. G., et al. 2010, A&A, 520, A95
Catelan, M. 2004, in IAU Colloq. 193: Variable Stars in the Local Group, eds. D. W. Kurtz, & K. R. Pollard, ASP Conf. Ser., 310, 113
Catelan, M. 2009, Ap&SS, 320, 261
Ciceri, S., Mancini, L., Southworth, J., et al. 2016, MNRAS, 456, 990
Clement, C. M., Muzzin, A., Dufton, Q., et al. 2001, AJ, 122, 2587
Cox, A. N., Hodson, S. W., & Clancy, S. P. 1983, ApJ, 266, 94
Cseresnjes, P. 2001, A&A, 375, 909
Draper, P. W. 2000, in Astronomical Data Analysis Software and Systems IX, eds. N. Manset, C. Veillet, & D. Crabtree, ASP Conf. Ser., 216, 615
Evans, D. F., Southworth, J., Maxted, P. F. L., et al. 2016, A&A, 589, A58
Figuera Jaimes, R., Arellano Ferro, A., Bramich, D. M., Giridhar, S., & Kuppuswamy, K. 2013, A&A, 556, A20
Figuera Jaimes, R., Bramich, D. M., Skottfelt, J., et al. 2016, A&A, 588, A128
Goldsbury, R., Richer, H. B., Anderson, J., et al. 2010, AJ, 140, 1830
Hamanowicz, A., Pietrukowicz, P., Udalski, A., et al. 2016, Acta Astron., 66, 197
Harpsøe, K. B. W., Jørgensen, U. G., Andersen, M. I., & Grundahl, F. 2012, A&A, 542, A23
Harris, W. E. 1996, AJ, 112, 1487
Ibata, R., Bellazzini, M., Chapman, S. C., et al. 2009, ApJ, 699, L169
Jerram, P., Pool, P. J., Bell, R., et al. 2001, in Sensors and Camera Systems for Scientific, Industrial, and Digital Photography Applications II, eds. M. M. Blouke, J. Canosa, & N. Sampat, SPIE Conf. Ser., 4306, 178
King, I. R. 1966, AJ, 71, 64
Kinman, T. D. 1959, MNRAS, 119, 134
Lafler, J., & Kinman, T. D. 1965, ApJS, 11, 216
Layden, A. C., & Sarajedini, A. 2000, AJ, 119, 1760
Lee, J.-W., & Carney, B. W. 1999, AJ, 118, 1373
Li, K., & Qian, S.-B. 2013, New Astron., 22, 57
Majewski, S. R., Skrutskie, M. F., Weinberg, M. D., & Ostheimer, J. C. 2003, ApJ, 599, 1082
Mancini, L., Giacobbe, P., Littlefair, S. P., et al. 2015, A&A, 584, A104
McDonald, I., Zijlstra, A. A., Sloan, G. C., et al. 2014, MNRAS, 439, 2618
McLaughlin, D. E., & van der Marel, R. P. 2005, ApJS, 161, 304
Milone, A. P. 2015, ArXiv e-prints [arXiv:1510.02578]
Monaco, L., Bellazzini, M., Ferraro, F. R., & Pancino, E. 2005, MNRAS, 356, 1396
Montiel, E. J., & Mighell, K. J. 2010, AJ, 140, 1500
Moskalik, P. 2013, in Stellar Pulsations: Impact of New Instrumentation and New Insights, eds. J. C. Suárez, R. Garrido, L. A. Balona, & J. Christensen-Dalsgaard, Astrophys. Space Sci. Proc., 31, 103
Netzel, H., Smolec, R., & Dziembowski, W. 2015, MNRAS, 451, L25
Oosterhoff, P. T. 1939, The Observatory, 62, 104
Pryor, C., & Meylan, G. 1993, in Structure and Dynamics of Globular Clusters, eds. S. G. Djorgovski, & G. Meylan, ASP Conf. Ser., 50, 357
Rosenberg, A., Recio-Blanco, A., & García-Marín, M. 2004, ApJ, 603, 135
Rosino, L. 1952, Mem. Soc. Astron. It. , 23, 49
Rosino, L., & Nobili, F. 1958, Mem. Soc. Astron. It., 29, 413
Samus, N. N., Durlevich, O. V., & et al. 2009, VizieR Online Data Catalog: II/25
Siegel, M. H., Dotter, A., Majewski, S. R., et al. 2007, ApJ, 667, L57
Sirianni, M., Jee, M. J., Benítez, N., et al. 2005, PASP, 117, 1049
Skottfelt, J., Bramich, D. M., Figuera Jaimes, R., et al. 2013, A&A, 553, A111
Skottfelt, J., Bramich, D. M., Figuera Jaimes, R., et al. 2015a, A&A, 573, A103
Skottfelt, J., Bramich, D. M., Hundertmark, M., et al. 2015b, A&A, 574, A54
Smith, H. A. 1995, Cambridge Astrophys. Ser., 27
Smith, N., Giltinan, A., O'Connor, A., et al. 2008, in Astrophys. Space Sci. Libr. 351, eds. D. Phelan, O. Ryan, & A. Shearer, 257
Smith, H. A., Catelan, M., & Kuehn, C. 2011, in RR Lyrae Stars, Metal-Poor Stars, and the Galaxy, Carnegie Obs. Astrophys. Ser. 5, ed. A. McWilliam, 17
Sollima, A., Cacciari, C., Bellazzini, M., & Colucci, S. 2010, MNRAS, 406, 329
Sollima, A., Cassisi, S., Fiorentino, G., & Gratton, R. G. 2014, MNRAS, 444, 1862
Soszyński, I., Udalski, A., Pietrukowicz, P., et al. 2011, Acta Astron., 61, 285
Soszyński, I., Udalski, A., Szymański, M. K., et al. 2014, Acta Astron., 64, 177
Southworth, J., Mancini, L., Tregloan-Reed, J., et al. 2015, MNRAS, 454, 3094
Street, R. A., Udalski, A., Calchi Novati, S., et al. 2016, ApJ, 819, 93
Udalski, A., Szymanski, M., Kaluzny, J., Kubiak, M., & Mateo, M. 1992, Acta Astron., 42, 253
Udalski, A., Szymański, M. K., & Szymański, G. 2015, Acta Astron., 65, 1
Wallerstein, G. 2002, PASP, 114, 689
Wilson, C. P. 1975, AJ, 80, 175
Wrobel, J. M., Greene, J. E., & Ho, L. C. 2011, AJ, 142, 113

[1] SUPA, School of Physics and Astronomy, University of St. Andrews, North Haugh, St Andrews, KY16 9SS, UK
e-mail: robertofiguera@gmail.com
[2] European Southern Observatory, Karl-Schwarzschild-Straße 2, 85748 Garching bei München, Germany
[3] Qatar Environment and Energy Research Institute (QEERI), HBKU, Qatar Foundation, Doha, Qatar
[4] Centre for Electronic Imaging, Dept. of Physical Sciences, The Open University, Milton Keynes MK7 6AA, UK
[5] Niels Bohr Institute and Centre for Star and Planet Formation, University of Copenhagen, Øster Voldgade 5, 1350 Copenhagen K, Denmark
[6] Space Telescope Science Institute, 3700 San Martin Drive, Baltimore, MD 21218, USA
[7] Dipartimento di Fisica "E. R. Caianiello", Università di Salerno, via Giovanni Paolo II 132, 84084 Fisciano, Italy
[8] Istituto Nazionale di Fisica Nucleare, Sezione di Napoli, 80126 Napoli, Italy

[9] NASA Exoplanet Science Institute, MS 100-22, California Institute of Technology, Pasadena CA 91125, USA
[10] Istituto Internazionale per gli Alti Studi Scientifici (IIASS), 84019 Vietri Sul Mare, Italy
[11] Max Planck Institute for Astronomy, Königstuhl 17, 69117 Heidelberg, Germany
[12] Yunnan Observatories, Chinese Academy of Sciences, 650011 Kunming, PR China
[13] Key Laboratory for the Structure and Evolution of Celestial Objects, Chinese Academy of Sciences, 650011 Kunming, PR China
[14] Korea Astronomy and Space Science Institute, Daejeon 305-348, Republic of Korea
[15] Finnish Centre for Astronomy with ESO (FINCA), University of Turku, Väisäläntie 20, 21500 Piikkiö, Finland
[16] Instituto de Astrofísica, Facultad de Física, Pontificia Universidad Católica de Chile, Av. Vicuña Mackenna 4860, 7820436 Macul, Santiago, Chile
[17] Department of Physics, Sharif University of Technology, PO Box 11155-9161 Tehran, Iran
[18] Astronomisches Rechen-Institut, Zentrum für Astronomie der Universität Heidelberg, Mönchhofstr. 12-14, 69120 Heidelberg, Germany
[19] Planetary and Space Sciences, Department of Physical Sciences, The Open University, Milton Keynes, MK7 6AA, UK
[20] Max-Planck-Institute for Solar System Research, Justus-von-Liebig-Weg 3, 37077 Göttingen, Germany
[21] Astrophysics Group, Keele University, Staffordshire, ST5 5BG, UK
[22] Las Cumbres Observatory Global Telescope Network, 6740 Cortona Drive, Suite 102, Goleta, CA 93117, USA
[23] Institut d'Astrophysique et de Géophysique, Université de Liège, Allée du 6 Août 9c, 4000 Liège, Belgium
[24] Dark Cosmology Centre, Niels Bohr Institute, University of Copenhagen, Juliane Maries vej 30, 2100 Copenhagen Ø, Denmark
[25] Department of Astronomy, Stockholm University, AlbaNova University Center, 106 91 Stockholm, Sweden
[26] Meteorologisches Institut, Universität Hamburg, Bundesstraße 55, 20146 Hamburg, Germany
[27] Universidad de Antofagasta, Unidad de Astronomía, Facultad Cs. Básicas, Av. U. de Antofagasta, 02800 Antofagasta, Chile
[28] 20 CITEUC – Centre for Earth and Space Science Research of the University of Coimbra, Observatório Astronómico da Universidade de Coimbra, 3040-004 Coimbra, Portugal
[29] Jodrell Bank Centre for Astrophysics, School of Physics and Astronomy, University of Manchester, Oxford Road, Manchester M139PL, UK
[30] Stellar Astrophysics Centre, Department of Physics and Astronomy, Aarhus University, Ny Munkegade 120, 8000 Aarhus C, Denmark

Appendix A: Additional tables and figures

Table A.1. Ephemerides and main characteristics of the variable stars in the field of globular cluster NGC 6715.

Var id (1)	Other id (2)	RA J2000 (3)	Dec J2000 (4)	Epoch HJD (5)	P d (6)	$I_{\rm median}$ mag (7)	$A_{i'+z'}$ mag (8)	N (9)	Type (10)
V112	–	18:55:02.010	–30:28:35.13	2 457 190.7419	100(1)	13.63	0.34	44	SR
V160	VC34; 37595	18:55:03.954	–30:28:29.83	2 457 189.7725	0.62813716(382)	17.65	0.75	40	RR0
V173	–	18:55:02.473	–30:29:00.04	2 457 206.6555	0.360284(152)	17.69	0.30	44	RR1
V181	VC28	18:55:02.395	–30:28:34.20	2 457 145.9107	0.877072(898)	17.60	0.87	42	RR0
V192	VC46; 37568	18:55:01.973	–30:29:02.27	2 456 784.9179	0.60035438(1060)	17.63	0.60	44	RR0
V212	VC35	18:55:03.777	–30:29:03.51	2 457 214.8470	0.202144(48)	17.59	0.79	42	E
V213	O16; VC40	18:55:02.126	–30:28:39.63	2 456 771.8623	0.286053(96)	17.95	0.64	44	RR1
V214	O16; VC39	18:55:02.964	–30:28:35.37	2 456 765.9179	0.305386(109)	16.97	0.45	44	RR1
V215	O16; VC25	18:55:02.701	–30:28:52.71	2 456 789.8857	0.307160(110)	17.45	0.34	44	RR1
V216	VC9	18:55:04.011	–30:28:37.73	2 457 292.6392	0.331073(128)	16.49	0.20	44	RR1
V217	O16	18:55:02.070	–30:29:03.41	2 457 205.7553	0.331556(128)	17.76	0.35	44	RR1
V218	–	18:55:03.556	–30:28:56.77	2 456 891.5200	0.348450(142)	16.92	0.20	44	RR1
V219	O16	18:55:03.233	–30:28:59.48	2 457 183.7770	0.382637(171)	17.21	0.24	44	RR1
V220	O16; VC4	18:55:03.197	–30:28:38.54	2 456 765.9102	0.388893(177)	16.86	0.27	44	RR1
V221	VC8	18:55:04.353	–30:28:51.16	2 456 846.9179	0.459608(247)	17.39	0.71	44	RR01
V222	–	18:55:02.504	–30:28:46.40	2 456 765.9179	0.465653(253)	17.70	0.70	44	RR0?
V223	O16; VC10	18:55:02.425	–30:28:45.20	2 456 823.8857	0.471901(260)	17.63	0.81	44	RR0
V224	VC20	18:55:03.549	–30:28:45.09	2 457 292.6392	0.482336(272)	16.16	0.27	44	RR0?
V225	VC37	18:55:03.862	–30:28:43.86	2 456 464.9081	0.483029(272)	17.28	0.35	44	RR1?
V226	–	18:55:03.948	–30:28:42.65	2 456 784.9179	0.497941(289)	16.39	0.36	44	RR0?
V227	37582	18:55:03.050	–30:28:35.81	2 457 190.7991	0.50805795(495)	17.66	0.90	44	RR0
V228	37575	18:55:02.757	–30:28:50.88	2 456 534.6709	0.52522562(844)	16.87	0.41	44	RR0
V229[a]	37597[b] ;	18:55:04.033	–30:28:58.20	2 456 788.9321	0.52679780(281)	16.38	0.28	41	RR0
V230	O16	18:55:03.637	–30:28:55.39	2 456 465.8700	0.532617(331)	16.04	0.29	44	RR0
V231	O16	18:55:02.894	–30:28:58.30	2 457 189.8090	0.534194(333)	17.80	0.83	44	RR0
V232	VC41	18:55:03.581	–30:28:47.60	2 456 543.5260	0.556536(362)	16.35	0.29	44	RR0
V233	VC30; 37591	18:55:03.735	–30:28:40.24	2 456 846.9179	0.55752742(766)	17.41	0.93	44	RR0
V234	O16; VC7	18:55:02.255	–30:28:37.13	2 457 206.6400	0.559765(366)	17.72	0.60	44	RR0
V235	–	18:55:03.411	–30:29:05.75	2 457 292.6392	0.566711(375)	17.41	0.69	43	RR0
V236	VC36; 37585	18:55:03.149	–30:28:34.86	2 457 152.8500	0.56847125(715)	16.53	0.28	44	RR0
V237	VC31; 37570	18:55:02.112	–30:28:44.40	2 456 435.8882	0.57985290(735)	17.57	0.65	44	RR0
V238	–	18:55:03.242	–30:28:42.94	2 456 846.9179	0.584918(399)	17.63	1.69	44	RR0
V239	O16	18:55:02.848	–30:29:06.91	2 457 189.8090	0.596179(432)	17.57	0.69	39	RR0
V240	37576	18:55:02.725	–30:28:30.46	2 456 909.5275	0.59629933(890)	17.06	0.54	43	RR0
V241	O16; VC1	18:55:04.190	–30:28:39.15	2 456 896.5087	0.602588(424)	17.79	0.65	44	RR0
V242	O16	18:55:02.756	–30:29:00.15	2 456 891.4700	0.604762(427)	16.23	0.16	44	RR0
V243	–	18:55:02.587	–30:28:38.62	2 456 770.8691	0.610170(435)	16.97	0.36	44	RR0
V244[a]	37581	18:55:03.031	–30:29:01.15	2 456 891.4945	0.61517949(819)	16.90	0.27	44	RR0
V245	VC26	18:55:02.849	–30:28:57.81	2 456 771.8623	0.626797(459)	17.68	0.47	44	RR0
V246[a]	37573	18:55:02.616	–30:28:40.91	2 457 207.8691	0.62879467(894)	16.11	0.06	42	RR0
V247	O16	18:55:02.826	–30:28:43.51	2 456 846.9179	0.650946(495)	16.86	0.42	44	RR0
V248	–	18:55:03.795	–30:28:54.42	2 457 258.7147	0.668967(522)	17.05	0.46	44	RR0
V249	–	18:55:03.226	–30:28:43.99	2 457 191.7238	0.673703(530)	15.91	0.21	44	RR0
V250	VC23; 37590	18:55:03.705	–30:29:00.36	2 456 543.5260	0.68064951(790)	17.54	0.58	44	RR0
V251	37579	18:55:02.876	–30:28:30.48	2 457 189.7725	0.68928616(716)	17.54	0.88	43	RR0
V252	37593	18:55:03.792	–30:29:07.83	2 457 189.8090	0.72866844(702)	17.28	0.50	17	RR0

Notes. Column 1 is the id assigned to the variable star; Col. 2 is a previously known id assigned to the stars (5 digit numbers correspond to OGLE identifications of the form OGLE-BLG-RRLYR-*NNNNN*; O16 indicates that the variable star was discovered independently by Hamanowicz et al. 2016, see note added in proof after our conclusions), Cols. 3 and 4 correspond to the right ascension and declination (J2000); Col. 5 is the epoch used; Col. 6 is the period measured in this work unless the variable is an OGLE star, in which case we use their period; Col. 7 is the median magnitude; Col. 8 is the peak-to-peak amplitude in the light curve; Col. 9 is the number of epochs; and Col. 10 is the classification of the variable. The numbers in parentheses indicate the uncertainty on the last decimal place of the period. [(a)] Epochs, periods, mean magnitudes, amplitudes, and classifications taken from OGLE database; [(b)] SPVSgr18550405-3028580; [(c)] SPVSgr18550386-3028593; [(d)] peak magnitude.

Table A.1. continued.

Var id (1)	Other id (2)	RA J2000 (3)	Dec J2000 (4)	Epoch HJD (5)	P d (6)	$I_{\rm median}$ mag (7)	$A_{i'+z'}$ mag (8)	N (9)	Type (10)
V253	37586	18:55:03.268	–30:28:28.69	2 457 206.6555	0.74391157(1160)	17.32	0.29	17	RR0
V254	O16	18:55:02.808	–30:28:49.69	2 456 436.8969	0.747628(652)	17.06	0.71	44	RR0
V255	O16; VC5	18:55:03.123	–30:28:37.99	2 456 765.8300	0.760088(674)	16.48	0.19	44	RR0
V256	O16	18:55:03.730	–30:28:44.94	2 456 784.9179	14.771(25)	14.72	0.71	44	CWA
V257	–	18:55:02.996	–30:28:43.18	2 456 823.8857	20.747(50)	14.04	0.09	44	SR
V258	–	18:55:03.732	–30:28:48.34	2 457 224.5000	37.980(168)	13.16	0.04	44	SR
V259	–	18:55:04.216	–30:28:49.91	2 456 464.9081	154(3)	13.30	0.45	44	SR
V260	–	18:55:03.170	–30:28:54.44	–	–	12.76	0.06	44	L
V261	–	18:55:03.399	–30:28:44.99	–	–	13.78	0.07	44	L
V262	O16	18:55:01.876	–30:28:43.79	–	–	13.99	0.07	40	L
V263	O16;[c]	18:55:03.877	–30:28:59.31	–	–	14.71	0.07	44	L
V264	–	18:55:03.753	–30:28:49.36	–	–	13.87	0.08	44	L
V265	–	18:55:02.987	–30:28:51.96	–	–	14.00	0.08	44	L
V266	–	18:55:03.458	–30:28:46.47	–	–	14.04	0.08	44	L
V267	–	18:55:03.463	–30:28:45.05	–	–	13.66	0.09	44	L
V268	–	18:55:02.998	–30:28:44.30	–	–	13.79	0.09	44	L
V269	–	18:55:03.712	–30:28:43.08	–	–	13.62	0.10	44	L
V270	O16	18:55:02.603	–30:28:48.92	–	–	13.70	0.11	44	L
V271	O16	18:55:04.004	–30:28:37.05	–	–	13.97	0.12	44	L
V272	–	18:55:03.065	–30:28:47.99	–	–	14.25	0.05	44	L
V273	O16	18:55:03.708	–30:28:35.30	–	–	13.40	0.15	44	L
V274	O16	18:55:03.833	–30:29:03.89	–	–	13.47	0.08	44	L
V275	O16	18:55:02.346	–30:28:43.40	–	–	13.67	0.16	44	L
V276	–	18:55:03.659	–30:28:50.52	–	–	14.06	0.16	44	L
V277	–	18:55:03.309	–30:28:49.79	–	–	13.71	0.19	44	L
V278	–	18:55:04.070	–30:28:49.79	–	–	13.13	0.33	44	L
V279	O16	18:55:04.045	–30:28:41.41	–	–	13.42	0.34	44	L
V280	O16	18:55:03.692	–30:28:52.01	–	–	13.25	0.46	44	L
V281	–	18:55:03.324	–30:28:47.26	–	–	16.71	0.45	44	NC
V282	–	18:55:03.010	–30:28:35.82	–	–	17.52	0.74	44	NC
V283	–	18:55:03.747	–30:28:53.88	–	–	16.97	0.76	44	NC
V284	O16; VC32	18:55:03.367	–30:28:37.97	–	–	17.14	0.94	44	NC
V285	O16; VC33	18:55:02.686	–30:28:32.48	–	–	17.52	0.55	44	NC
V286	O16	18:55:03.536	–30:28:51.06	–	–	15.04[d]	–	43	NC
V287	O16	18:55:03.373	–30:28:35.86	–	–	–	–	44	NC
V288	–	18:55:03.412	–30:28:52.76	–	–	–	–	44	NC
V289	O16	18:55:02.904	–30:28:39.89	–	–	–	–	42	NC
V290	O16	18:55:03.475	–30:29:06.23	–	–	–	–	39	NC
V291	O16; VC27	18:55:03.258	–30:28:41.09	–	–	–	–	42	NC

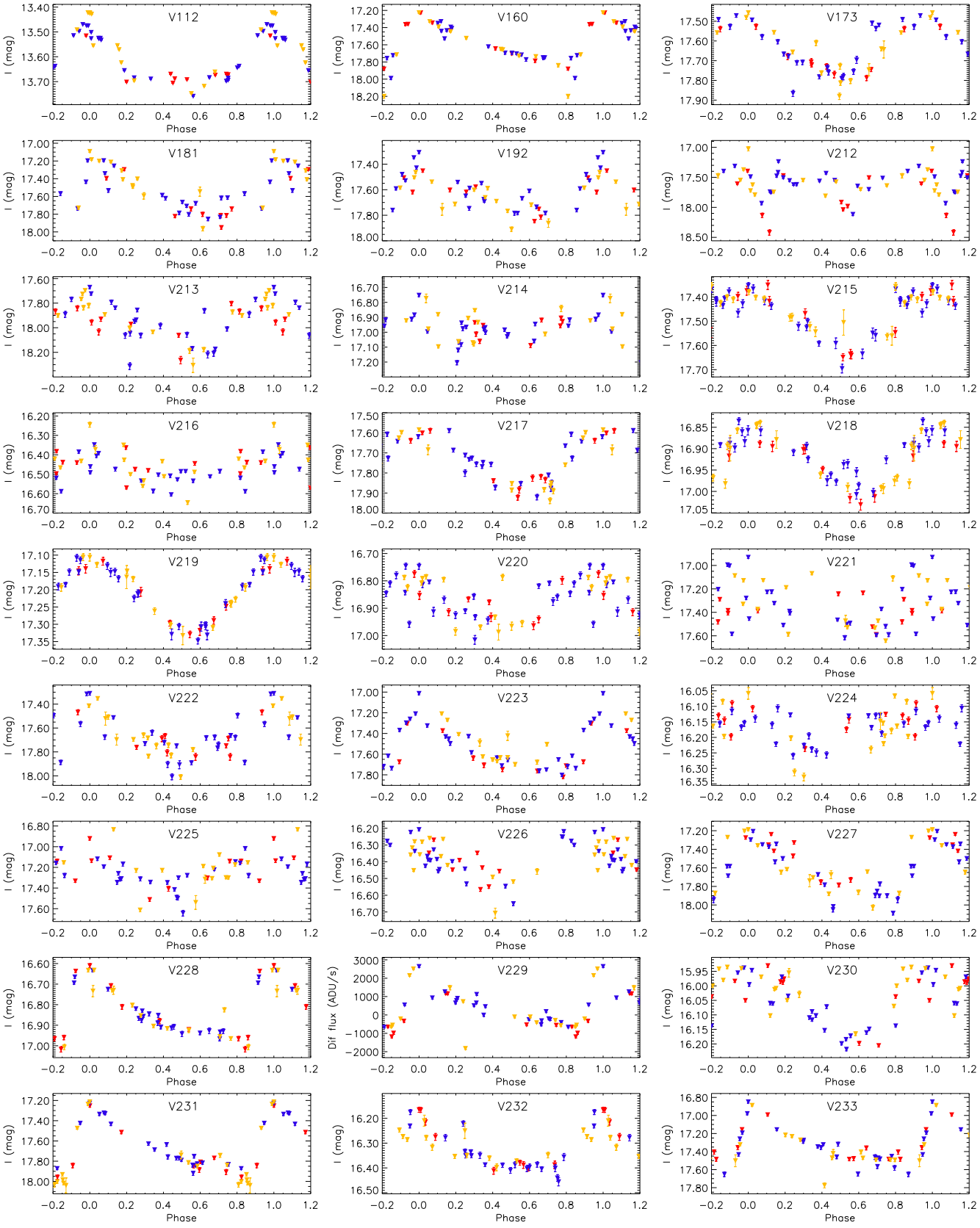

(a)

Fig. A.1. Light curves of the known and new variables discovered in globular cluster NGC 6715. Red, blue, and yellow triangles correspond to the data obtained during the years 2013, 2014, and 2015, respectively. For V229, V244, V246, V286-V291, we plot the quantity $f_{\rm diff}(t)/p(t)$ since a reference flux is not available.

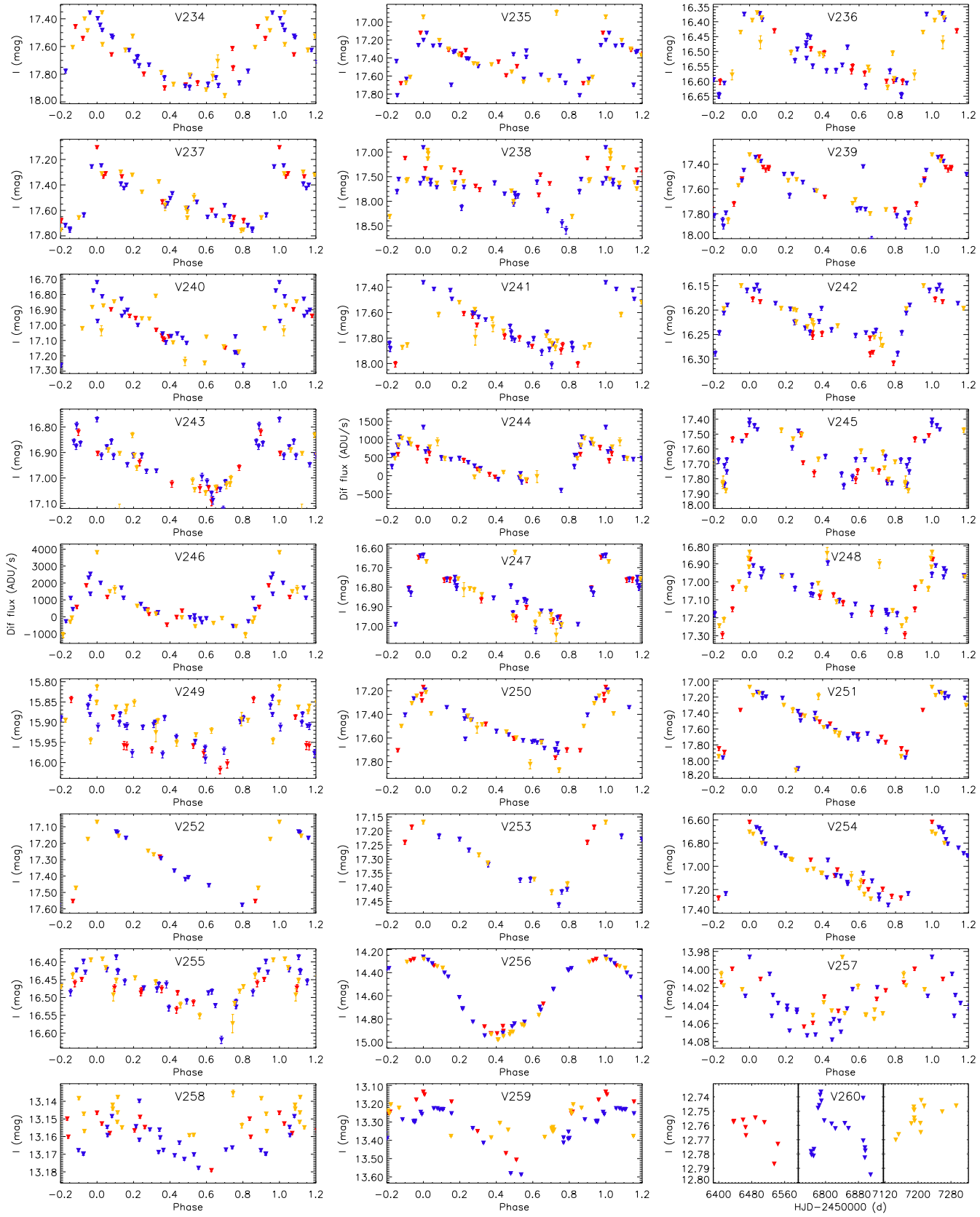

(b)

Fig. A.1. continued.

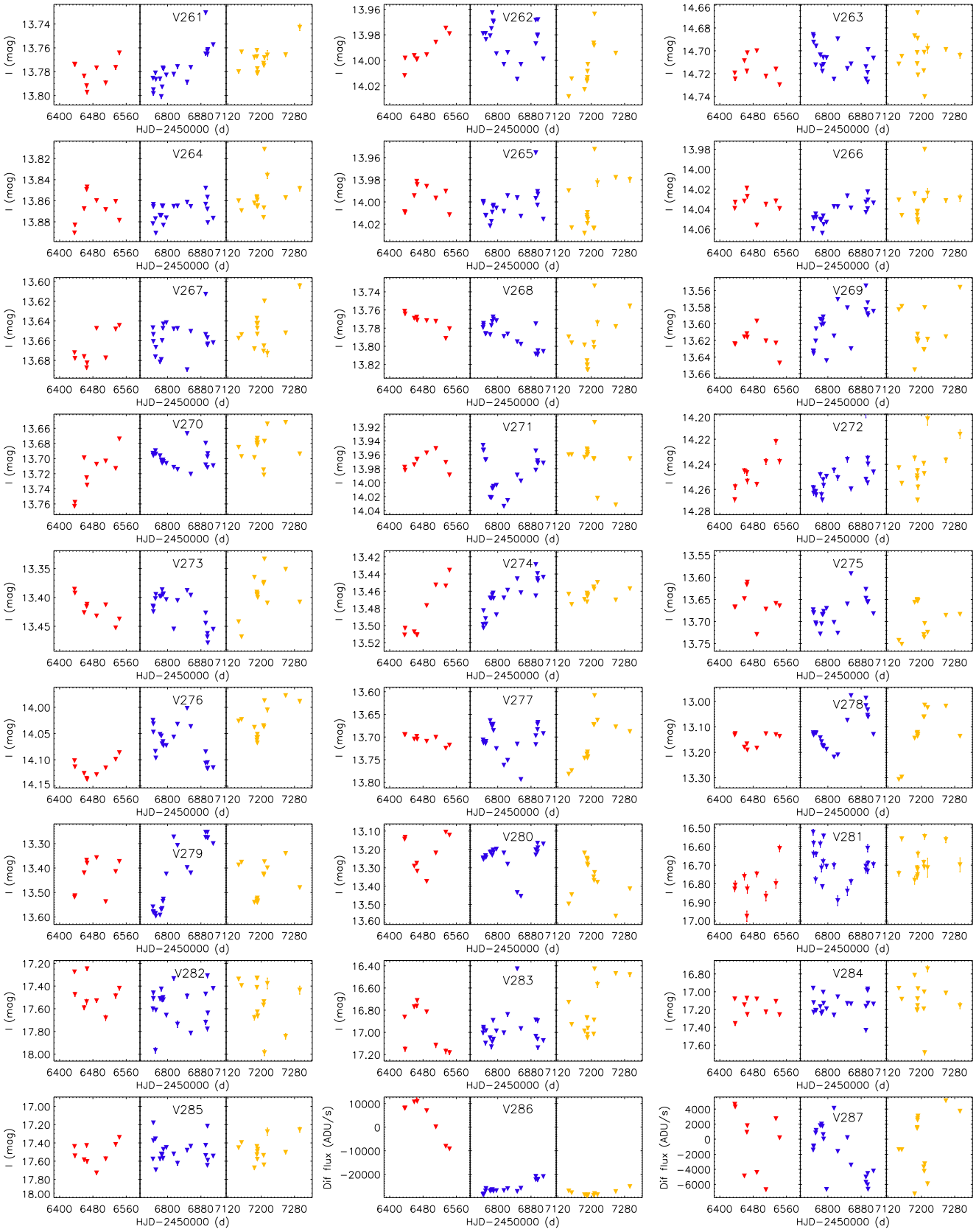

(c)

Fig. A.1. continued.

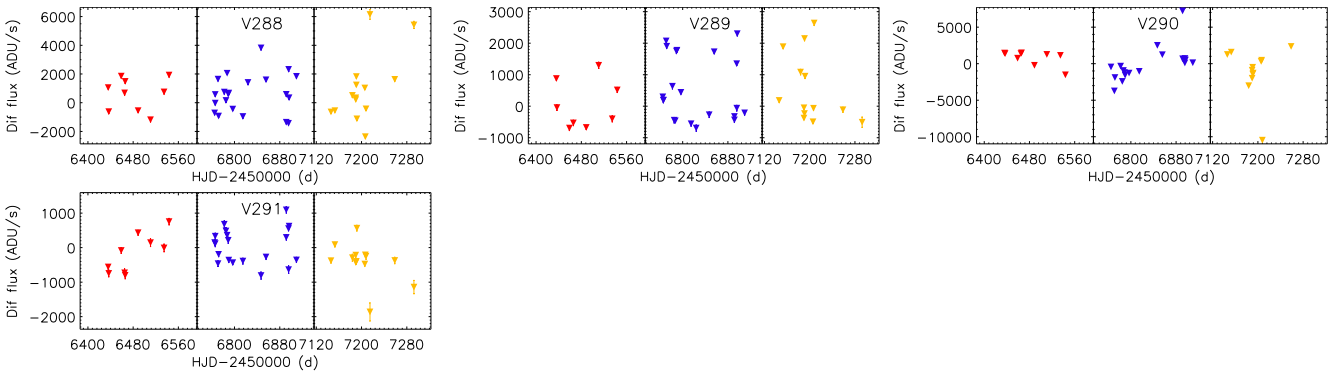

(d)

Fig. A.1. continued.

Appendix B: Cross-identification between variables

Table B.1. Cross-identification between the RR Lyrae variables listed by the CVSGGC (Clement et al. 2001), the variable star candidates from Montiel & Mighell (2010), and the OGLE RR Lyrae stars (Soszyński et al. 2014).

CVSGGC id	OGLE id (OGLE-BLG-)	Montiel id	CVSGGC id	OGLE id	Montiel id	CVSGGC id	OGLE id	Montiel id
V3	RRLYR-37571		V92	RRLYR-37611		V186	RRLYR-37546	
V4	RRLYR-37540		V93	RRLYR-37567		V188	RRLYR-37584	
V5	RRLYR-37518		V94	RRLYR-37634		V192	RRLYR-37568	VC46
V6	RRLYR-37655		V95	RRLYR-37560	VC13	V193	RRLYR-37605	
V7	RRLYR-37620		V97	RRLYR-37607		V194	RRLYR-37574	
V12	RRLYR-37511		V98	RRLYR-37637		V227	RRLYR-37582	
V15	RRLYR-37649		V118	RRLYR-37660		V228	RRLYR-37575	
V28	RRLYR-37623		V119	RRLYR-37654		V229	RRLYR-37597	
V29	RRLYR-37519		V120	RRLYR-37638		V233	RRLYR-37591	
V31	RRLYR-37528		V121	RRLYR-37635		V236	RRLYR-37585	
V32	RRLYR-37514		V122	RRLYR-37632		V237	RRLYR-37570	
V33	RRLYR-37631		V123	RRLYR-37583		V240	RRLYR-37576	
V34	RRLYR-37541		V124	RRLYR-37628		V244	RRLYR-37581	
V35	RRLYR-37533		V125	RRLYR-37613		V246	RRLYR-37573	
V36	RRLYR-37648		V126	RRLYR-37600		V250	RRLYR-37590	
V37	RRLYR-37617		V127	RRLYR-37580	VC2	V251	RRLYR-37579	
V38	RRLYR-37538		V128	RRLYR-37551		V252	RRLYR-37593	
V39	RRLYR-37527		V129	RRLYR-37526	VC17	V253	RRLYR-37586	
V40	RRLYR-37543		V130	RRLYR-37549		–	RRLYR-37578	VC38
V41	RRLYR-37647		V131	RRLYR-37525				
V42	RRLYR-37626		V132	RRLYR-37555				
V43	RRLYR-37516		V133	RRLYR-37550				
V44	RRLYR-37599		V136	RRLYR-37513				
V45	RRLYR-37646		V137	RRLYR-37612				
V46	RRLYR-37552	VC44	V138	RRLYR-37610				
V47	RRLYR-37554		V139	RRLYR-37596				
V48	RRLYR-37659		V140	RRLYR-37572				
V49	RRLYR-37532		V141	RRLYR-37558				
V50	RRLYR-37640		V142	RRLYR-37545	VC15			
V51	RRLYR-37657		V143	RRLYR-37534				
V52	RRLYR-37636		V147	RRLYR-37602				
V54	RRLYR-37521		V148	–	VC45			
V55	RRLYR-37651		V151	RRLYR-37517				
V57	RRLYR-37666		V152	RRLYR-37615				
V58	RRLYR-37630		V158	RRLYR-37539				
V59	RRLYR-37512		V159	RRLYR-37589				
V60	RRLYR-37509		V160	RRLYR-37595	VC34			
V61	RRLYR-37547		V161	RRLYR-37616				
V62	RRLYR-37531		V162	RRLYR-37592	VC11			
V63	RRLYR-37553		V163	RRLYR-37604	VC12			
V67	RRLYR-37587		V164	RRLYR-37564	VC14			
V69	RRLYR-37505		V165	RRLYR-37609				
V74	RRLYR-37645		V168	RRLYR-37619				
V76	RRLYR-37529	VC47	V172	RRLYR-37614				
V77	RRLYR-37524		V174	RRLYR-37608				
V78	RRLYR-37629		V176	RRLYR-37618				
V80	RRLYR-37624		V177	RRLYR-37556				
V82	RRLYR-37548		V178	RRLYR-37562				
V83	RRLYR-37522		V179	RRLYR-37557	VC18			
V84	RRLYR-37577		V180	RRLYR-37588				
V85	RRLYR-37569		V181	–	VC28			
V87	RRLYR-37641		V182	RRLYR-37561				
V88	RRLYR-37515		V183	RRLYR-37603				
V89	RRLYR-37530		V184	RRLYR-37559				
V90	RRLYR-37622		V185	RRLYR-37563				